A Novel Method of Semiconductor Device Measurements*

T. E. EVERHART,† O. C. WELLS,†† AND R. K. MATTA†††

Summary--Electrical signals induced in semiconductor devices by a high-resolution scanning electron beam have been used to determine the boundaries of doped (p or n) regions, even when these boundaries lie beneath passivating oxide layers, or beneath evaporated metal leads. The uniformity of planar junctions lying beneath the device surface can also be ascertained by this method, and the junction depth can be estimated by comparing measurements made at different electron beam voltages. The spatial resolution of this technique is limited by the penetration and scattering of electrons in the device material; these scattering effects are discussed, and representative micrographs showing resolutions of a few microns are presented, as well as various quantitative measurements related to the method.

---

* The experiments described in this paper were performed at the Westinghouse Research Laboratories, Pittsburgh 35, Pennsylvania, and were presented at the 1963 Professional Technical Group on Electron Devices Meeting in Washington, D. C.

† Department of Electrical Engineering, University of California, Berkeley 4, California.

†† CBS Laboratories, Stamford, Connecticut.

††† Westinghouse Research Laboratories, Pittsburgh 35, Pennsylvania.

I. INTRODUCTION

As semiconductor devices are made smaller and smaller, their electrical evaluation becomes increasingly difficult. This paper describes a method of measurement which obviates most mechanical contact with the device surface, which is capable of submicron resolution, and which can determine the relative potential of different areas of the device surface. This method, essentially that of scanning electron microscopy, has been known for many years.[1-6] However, its application to passivated integrated circuits has only recently been described,[7-9] and qualitative results shown in the form of micrographs of the device surface.

In this method a very small diameter electron beam is scanned over the surface of an integrated circuit. The resulting secondary electrons are collected and provide a video signal which modulates the intensity of a synchronously scanned cathode-ray tube. Alternatively electron-beam-induced currents and voltages from the integrated circuit itself may be used as a video signal to provide supplementary information about the sample being examined. The emphasis of this paper is on electrical signals induced in a semiconductor device by scanning electron beam bombardment and on certain measurements which may be performed using these electrical signals.

In the work reported here the final electron spot diameter at the object was a few tenths of a micron, although spot diameters smaller than a hundred angstrom units have been achieved.[10] In order to achieve such small spot diameters, the beam current must necessarily be small, from 10^{-8} to 10^{-11} amperes in these experiments. The accelerating voltages ranged from 5 to 40 kv, which is far below the threshold values necessary to displace atoms from their correct position in the lattice.[11] Therefore, no Frenkel defects are caused by the electron beam used in these experiments.

II. ELECTRON PENETRATION AND SCATTERING EFFECTS

The penetration and scattering of a monoenergetic electron beam incident on a solid target has received considerable theoretical and experimental attention over the past few decades, but is not yet completely understood. The primary electrons penetrating into the solid may lose energy by exciting individual electrons within the solid to higher energy levels, or by ionizing them,[12] and by collective interactions with electrons in the solid which result in plasma oscillations.[13] Scattering is produced by collisions with atomic nuclei, tightly bound atomic electrons, valence electrons and conduction electrons. Scattering has been studied experimentally by measurements on backscattered electrons (secondary electrons with energies >50 ev),[14,15] measurements on "true" secondary electrons (energies <50 ev),[16,17] penetration through thin films,[18-22] and electroluminescence.[23,24] One important energy-loss mechanism for primary electrons bombarding semiconductors or insulators is the excitation of valence electrons into the conduction band, generating hole-electron pairs.[25-30] These carriers can increase the conductivity of insulators by many orders of magnitude; this effect is generally called electron-beam-induced conductivity (EBIC), and is also quite noticable in semiconductors, especially if the carriers are generated near a reverse-biased junction, or in its depletion layer.[26,27,29]

If quantitative measurements on p-n junction devices are to be performed using electron-beam-induced currents (EBI currents), the density of hole-electron pairs generated by the electron beam must be known as a function of position relative to the bombarded point on the target surface. It may be assumed that the generated carrier density is proportional to the primary electron-beam energy dissipated per unit volume.[17] This quantity has been studied by Ehrenberg and co-workers;[23] their results seem to vary from those reported by Grün[24] for gases, and extended by Schumacher and Mitra[31] to solids. Thus the exact distribution

of primary electron beam energy dissipated per unit volume does not appear to be known as a function of position in the target at present. However, all the incident beam energy is lost within a hemisphere centered at the point of impact, and having a radius equal to the maximum range of electrons in the material. Most of the energy is dissipated within a smaller concentric hemisphere with a radius equal to the practical range. The maximum and practical ranges of electrons in Silicon is shown in Fig. 1. It follows that a 10 kv electron beam of 0.1μ diameter incident on a Silicon target will generate hole-electron pairs within a 1μ hemisphere centered at the point of impact. For a 16 kv beam, the hemisphere will be approximately 2μ in radius. Since the resolution which can be achieved in scanning electron micrographs derived from electron-beam-induced voltages and currents will be related to (and generally limited by) this scatter, the distribution of energy dissipation with distance inside the target is of considerable importance for this work. Using specially fabricated targets and techniques related to those discussed in the next section, it may prove possible to measure transverse scatter with more accuracy than has hitherto been possible.

The energy needed to generate hole-electron pairs in the highly-doped silicon devices studied here was approximately 5 ev of incident energy for each pair. Thus a 15 kv electron excites about three thousand hole-electron pairs in these devices. The minority carriers diffuse away from the point of generation, and if they cross a p-n junction before recombining, an EBI current across that junction results. The maximum EBI current occurs when the beam energy is dissipated in or near the depletion layer, and is a measure of the pair production. The variation of the EBI current with distance of the electron probe from the junction is a measure of the carrier diffusion length.

In a multi-layer structure such as is shown in Fig. 2, the electrons may not penetrate into the semiconductor region at all, since they may lose all their energy in the aluminum leads or silicon oxide passivation layer. In Fig. 2 three different electron beam energies have been assumed.

For the lowest energy chosen, the electron beam penetrates only into the emitter region of the semiconductor. The next higher energy beam penetrates both the base and the emitter region, and the highest energy electrons chosen penetrate all three regions of the semiconductor device. However, because of the geometry, the amount of energy available for carrier generation is different in the various regions; for example, more carriers are produced near the emitter-base junction in Fig. 2 than near the base-collector junction. Therefore one would expect the EBI current across the emitter-base junction to be larger than the EBI current across the base-collector junction in the absence of applied bias. By properly biasing the collector, base, and emitter junctions, photo-transistor action can be obtained, using the electron beam as a source of carriers.

III. EXPERIMENTAL RESULTS

In this section, experimental results illustrating the penetration and scattering effects are presented as well as measurements on hole-electron pair creation. All these results were obtained with monolithic silicon passivated integrated circuits. While these experiments represent typical measurements which may be performed using this method, they are not meant to be exhaustive.

Fig. 3 shows four scanning electron micrographs. Micrograph (a) was produced by the secondary electron video signal only, when a bias was applied to the collector, base, and emitter of the passivated transistor. The diffusion beneath the masking oxide during fabrication is clearly shown in this micrograph and may be a useful measurement to the device engineer in its own right. Micrograph (b) was obtained by mixing the "photovoltage"* generated by the scanning electron beam with the

* The term "photovoltage" as used in this section refers to the voltage generated by EBI currents across a one megohm resistor external to the circuit under test, and connected between the circuit and ground.

secondary electron video signal. Note that the photovoltage darkens the micrograph; the effect is more pronounced near the base-emitter junction and the base-collector junction because almost all the carriers generated in the depletion layer where the junctions intercept the surface contribute to the EBI current. Conversely, carriers generated near the center of the base region have to diffuse to the collector-base junction before they can produce an EBI current. This micrograph was taken at a primary beam voltage of 12 kv, and no penetration of the emitter lead is apparent.

Micrographs (c) and (d) are of the same device, taken at beam voltages of 16 and 20 kv, respectively. The peak value of the photovoltage signal was held constant in these comparison micrographs. Note that penetration through the emitter aluminum evaporated lead (see arrow) has started to take place at 16 kv, but no penetration through the emitter region is yet noticeable. At 20 kv, however, appreciable penetration through the emitter region into the base has taken place, causing both the base and the emitter to be darkened.

Transverse penetration of the primary beam, which increases with increasing beam energy, is believed responsible for the increased displacement of the boundary of the photovoltage-darkened zone from the edge of the masking oxide; in micrograph 3(c) taken with a 16 kev electron beam, the darkened photovoltage zone starts approximately 2.5μ from the edge of the silicon oxide mask, whereas in micrograph 3(d), taken with a 20 kev electron beam, the edge of this zone is displaced approximately 4μ from the edge of the masking silicon oxide. Both of these micrographs should be compared with micrograph 3(a), where the junction position is estimated to be approximately 1.5μ from the edge of the masking silicon oxide. These results indicate that the secondary electron video signal produced a higher resolution micrograph for the purpose of locating junctions than does the photovoltage signal; more quantitative evidence for this conclusion is presented below.

It is also possible to measure these changes quantitatively by recording the video signals; Fig. 4 shows the results of such a quantitative measurement. The device shown in Fig. 4 was studied rather intensively

because of the peculiarity located in the base region, which is clearly seen in the micrograph. Both the video signal, consisting of the secondary electron signal mixed with the photovoltage signal, and the photovoltage signal alone were recorded as the electron beam swept horizontally across the line indicated by the arrows on the micrograph. The top trace of the chart recorder shows the video signal, which can be correlated to the intensity of the micrograph, negative-going signals being dark, and positive-going signals being light. The recording shows two successive lines of the scanned raster. The photovoltage is similarly recorded in the bottom trace. Here a positive-going signal appears dark on the micrograph and zero signal means no photovoltage is generated. The relative minimum in photovoltage corresponds to the light area in the center of the micrograph.

In Fig. 5 the photovoltage is plotted versus the beam power in microwatts. These data were obtained by setting the beam voltage to a given value, and then changing the beam current and monitoring the variation in the photovoltage with beam current. However, by plotting the points versus beam power, more universal curves are obtained. The 16 kv and the 23.8 kv curves coincide over much of their length; the 9.8 kv curve is somewhat lower because at the point where the curve was monitored a substantial fraction of the 9.8 kv beam energy was dissipated in the oxide covering the junction. The curves saturate at slightly different values of ordinate and abscissa, and at a relatively high value of the photovoltage. The important point about a curve of this sort is not that it is linear (as one would expect), or that it is unique, but that it can be obtained for any specific point on the surface of an integrated circuit, and therefore quantitative information about any specific point on the circuit can be correlated with the micrographs. This has not been possible in the past.

Fig. 6 shows EBI current across a reverse-biased junction plotted versus beam power. Again, linear curves were obtained for specific points on a given surface. The lines on this figure are drawn at an accurate 45^{o} angle which corresponds to a linear increase in induced current with beam

power. There is a tendency for the experimental data to be slightly below the line at the higher powers, and slightly above the line at the lower powers. No saturation effects are present or expected in these curves.

Fig. 7 shows the induced current gain, defined as the induced current crossing a junction divided by the incident electron beam current. When the beam is incident on a collector-base junction covered only by a passivating oxide layer, the collector-oxide curve is obtained. Note that there is a threshold of energy below which the beam does not penetrate the oxide and hole-electron pairs are not generated in the semiconductor material. Above this point, however, the curve increases; initially, as both the number of electrons penetrating through the oxide and their average energy is increasing, the rise is more rapid. At higher voltages, when the average energy of the electrons penetrating the oxide is increasing, but the number is essentially constant, the slope is somewhat less. The circle and triangle curves shown in Fig. 7 were taken from the same chart recording, but correspond to different points on the specimen, namely areas beneath an aluminum-base contact and beneath an aluminum-emitter contact respectively. Slightly more beam energy is required to produce a signal beneath the emitter contact than beneath the base contact. These curves also appear linear above a given current gain and may be extrapolated back to the voltage axis. The point where the extrapolated line cuts the beam voltage axis may be used to deduce the thickness of the aluminum and base contacts and the collector oxide in this device following the method of Schumacher and Mitra,[31] and taking into account the discussion of Kanter and Sternglass.[21] Until further calibration measurements are completed, the accuracy possible in determining these thicknesses is only 20 to 30 percent.

The resolution of this technique is limited by the diameter of the scanning electron beam, by scattering effects in the material being examined, and by signal-to-noise considerations.[5] Pease[10] at Cambridge University, has demonstrated electron beam spot diameters less than

100A in diameter, and resolutions approaching 100A using the secondary electron video signal. The location of p-n junctions on bare gallium phosphide to within 0.2 microns has been demonstrated by Everhart,[32] also using the secondary electron video signal.

We have studied the location of p-n junctions covered by passivating layers of silicon oxide, making quantitative measurements on the secondary electron video waveform, and on the electron-beam-induced photovoltage. A typical result is shown in Fig. 8 where the velocity of scan on the specimen surface was approximately 100μ /sec. The recorded curves of video signal vs. position as the electron beam is scanned over a reverse-biased junction closely resemble an integrated gaussian curve. Thus the ordinate in Fig. 8 is taken as the distance required for the recorded trace to rise from 0.16 to 0.84 of its final value, a distance which corresponds to twice the standard deviation of the gaussian curve. The integrated gaussian interpretation is not so convincing for the photovoltage traces, but has been used as a consistent method of reducing the recorded data. The curves shown here were obtained for a 0.2 micron thick silicon oxide layer. From similar data on thicker oxide layers, the rise distance of the collected secondary electrons seems almost independent of the oxide thickness. The photovoltage rise-distance increases with increasing oxide thickness, although the slope of rise distance vs. beam voltage decreases somewhat. It should be emphasized that these data are subject to error, due to the assumptions listed above and to the error inherent in manually reducing the recorded traces to the curves plotted here; for this reason, Fig. 8 must be considered a tentative result.

IV. DISCUSSION

A meaningful measurement generally should not appreciably perturb the system being observed. Electron beam bombardment will heat semiconductors, whose electrical properties are quite temperature sensitive, and will also generate hole-electron pairs, thus altering the

equilibrium conditions which existed before the beam struck the sample . Since in the work described in Sec. III, the electron beam was always moving across the sample surface, any calculation assuming a stationary beam should predict larger temperature rises and larger electron-beam generated carrier densities than will occur in practise. A sample calculation in which a stationary one microwatt electron beam strikes a silicon wafer, and the power is dissipated within a radius of one micron from the impact point reveals that considerably less than a one degree Centigrade temperature increase should be expected. A similar calculation for generated carrier densities in silicon which assumes a stationary beam and no recombination (the carriers leave the bombarded region by diffusion only) predicts that maximum carrier densities of the order of $10^{14} cm^{-3}$ might be expected. This number is larger than the carrier densities in intrinsic silicon by approximately three orders of magnitude. While recombination will tend to reduce this value, the maximum generated density of minority carriers in doped material may be orders of magnitude above the normal minority carrier density, and may even approach the majority carrier density.

The integrated circuit is a very complicated structure to understand exactly, consisting as it does of differently doped planar layers of single-crystal silicon (probably having a high density of crystallographic imperfections, such as dislocations[33]). Recombination and trapping centers located in the bulk, at interfaces between different planar regions, and at the device surface will greatly affect the measurements reported in this paper. Alternatively, controlled experiments using electron beams which are pulsed or scanned may provide new information on these topics.* Preliminary measurements have shown that a measure of the diffusion length, can be obtained using this technique. Pulse measurements should lead to a direct measure of carrier lifetime. Factors which complicate these

* Recent work by Lander, et al., [34] for example, has imaged dislocation networks on silicon surfaces using essentially this method.

measurements, such as excess charge introduced by the electron beam, possible charging of the passivating oxide layer, and surface contamination, must be assessed, and either eliminated, or taken into account when performing quantitative measurements more sophisticated than those presented here. This paper has attempted to provide some of the background information necessary to exploit this technique, as well as to show certain results already obtained by using it.

V. ACKNOWLEDGMENTS

The authors wish to acknowledge helpful technical discussions and encouragement from several colleagues at both the Westinghouse Research Laboratories and at the University of California. One of us (TEE) wishes to express appreciation to the Westinghouse Research Laboratories for support during an industrial leave of absence from the University of California, when the measurements reported here were performed.

This work was supported by the Electronics Technology Division, Aeronautical Systems Division, United States Air Force, Wright-Patterson Air Force Base, Ohio, under Contract No. AF 33(657)-9897.

REFERENCES

1. V. K. Zworykin, G. A. Morton, E. G. Ramberg, J. Hillier, and A. W. Vance, Electron Optics and the Electron Microscope, J. Wiley and Sons, Inc., New York; 1945.
2. D. McMullan, Proc. Inst. Elec. Engrs., Vol. 100 (II) p. 245; 1953.
3. K. C. A. Smith and C. W. Oatley, Brit. J. Appl. Phys., Vol. 6, p. 391; 1955.
4. T. E. Everhart, K. C. A. Smith, O. C. Wells, and C. W. Oatley, Proceedings of the Fourth International Conference on Electron Microscopy, Berlin, 1958, Springer-Verlag, Berlin, p. 269; 1960.
5. T. E. Everhart, O. C. Wells, and C. W. Oatley, J. Electronics Control, Vol. 7, p. 97; 1959.
6. K. C. A. Smith, Encylopedia of Microscopy, (G. L. Clark, ed.) Reinhold Publishing Corp., New York, p. 241; 1961.
7. I. M. Mackintosh, Abstract #118, Electrochem. Soc. Fall Meeting, New York; 1963.
8. T. E. Everhart, O. C. Wells, and R. K. Matta, J. Electrochem. Soc., to be published in August 1964.
9. O. C. Wells, T. E. Everhart, and R. K. Matta, Abstract #120, Electrochem Soc. Fall Meeting, New York; 1963.
10. F. Pease, Cambridge University, private communication.
11. J. J. Loferski and P. Rappaport, Phys. Rev., Vol. 100, p. 1261; 1955.
12. L. Marton, Rev. Modern Phys., Vol. 28, p. 172; 1956.
13. D. Pines, Idem., Vol. 28, p. 184; 1956.
14. E. J. Sternglass, Phys. Rev., Vol. 95, p. 345; 1954.
15. H. Kanter, Ann. Physik., Vol. 20, p. 144; 1957.
16. A. J. Dekker, Solid State Phys. (F. Seitz and D. Turnbull, eds.), Academic Press, New York, Vol. 6, p. 251; 1958.

17. H. Kanter, Phys. Rev., Vol. 121, p. 677; 1961.

18. H. A. Bethe, Ann. Physik., Vol. 7, p. 325; 1930.

19. A. F. Makhov, Fiz. Tverd. Tela., Vol. 2, p. 2161; 1960.

20. H. Kanter, Phys. Rev., Vol. 121, p. 461; 1961.

21. H. Kanter and E. J. Sternglass, Idem., Vol. 126, p. 620; 1962.

22. A. Y. Vyatskin and A. N. Polyankevich, Fiz. Tverd. Tela., Vol. 4, p. 1038; 1962.

23. W. Ehrenberg and J. Franks, Proc. Phys. Soc., B, Vol. 66, p. 1057; 1953; W. Ehrenberg and D. E. N. King, Idem., Vol. 81, p. 751; 1963.

24. A. E. Grün, Z. Naturforsch., Vol. 12a, p. 89; 1957.

25. N. B. Gornyi, Fiz. Tverd. Tela., Vol. 3, p. 698; 1961.

26. W. L. Brown, IRE Trans., Vol. NS-8, p. 2; 1961.

27. R. L. Williams and P. P. Webb, RCA Rev., Vol. 23, p. 29; 1962.

28. K. G. McKay and K. B. McAfee, Phys. Rev., Vol. 91, p. 1079; 1953.

29. A. V. Brown, IEEE Trans., Vol. ED-10, p. 8; 1963.

30. E. W. Billington and W. Ehrenberg, Proc. Phys. Soc., Vol 78, p. 845; 1961.

31. B. W. Schumacher and S. S. Mitra, Proc. 1962 Electronics Components Conference, Washington, D.C.; May 1962.

32. T. E. Everhart, Contrast Formation in the Scanning Electron Microscope, (PhD. Dissertation, Cambridge University), p. 122; 1958.

33. G. H. Schwuttke, paper presented at the 1963 Electron Devices Meeting, Washington, D. C., sponsored by IEEE, PTG-ED.

34. J. J. Lander, H. Schreiber, Jr., T. M. Buck, and J. R. Mathews, Appl. Phys. Lett., Vol. 3, p. 206; December 1963.

FIGURE CAPTIONS

Fig. 1. Range in silicon vs. primary beam voltage.

Fig. 2. Cross-sectional schematic of integrated circuit showing electron penetration.

Fig. 3. (a) Secondary electron video signal;
V_B = - 1v, V_c = + 2v, V_E = 0v
Beam voltage = 16 kv.
(b) Photovoltage mixed with secondary electron video signal;
V_B = photovoltage, V_C = + 1v, V_E = 0;
Beam voltage = 12 kv.
(c) Conditions as in (b)
Beam voltage = 16 kv.
(d) Conditions as in (b)
Beam voltage = 20 kv.
Scanning electron micrographs of an integrated circuit, illustrating the variation of the photovoltage signal with beam voltage.

Fig. 4. (a) Photovoltage mixed with video signal; collector-emitter bias = 4v. Beam voltage = 16 kv.
(b) Recorded video waveform and photovoltage of (a) at indicated horizontal line.
Scanning electron micrograph and recorded video and photovoltage waveforms, illustrating one method of obtaining permanent quantitative records.

Fig. 5. Photovoltage vs. beam power, with beam voltage as a parameter.

Fig. 6. Electron-beam-induced current vs. beam power, with beam voltage as a parameter.

Fig. 7. Current gain vs. beam voltage at different points on an integrated circuit.

Fig. 8. Rise distance of secondary electron video signal and photovoltage signal of the illustrated test sample vs. beam voltage.

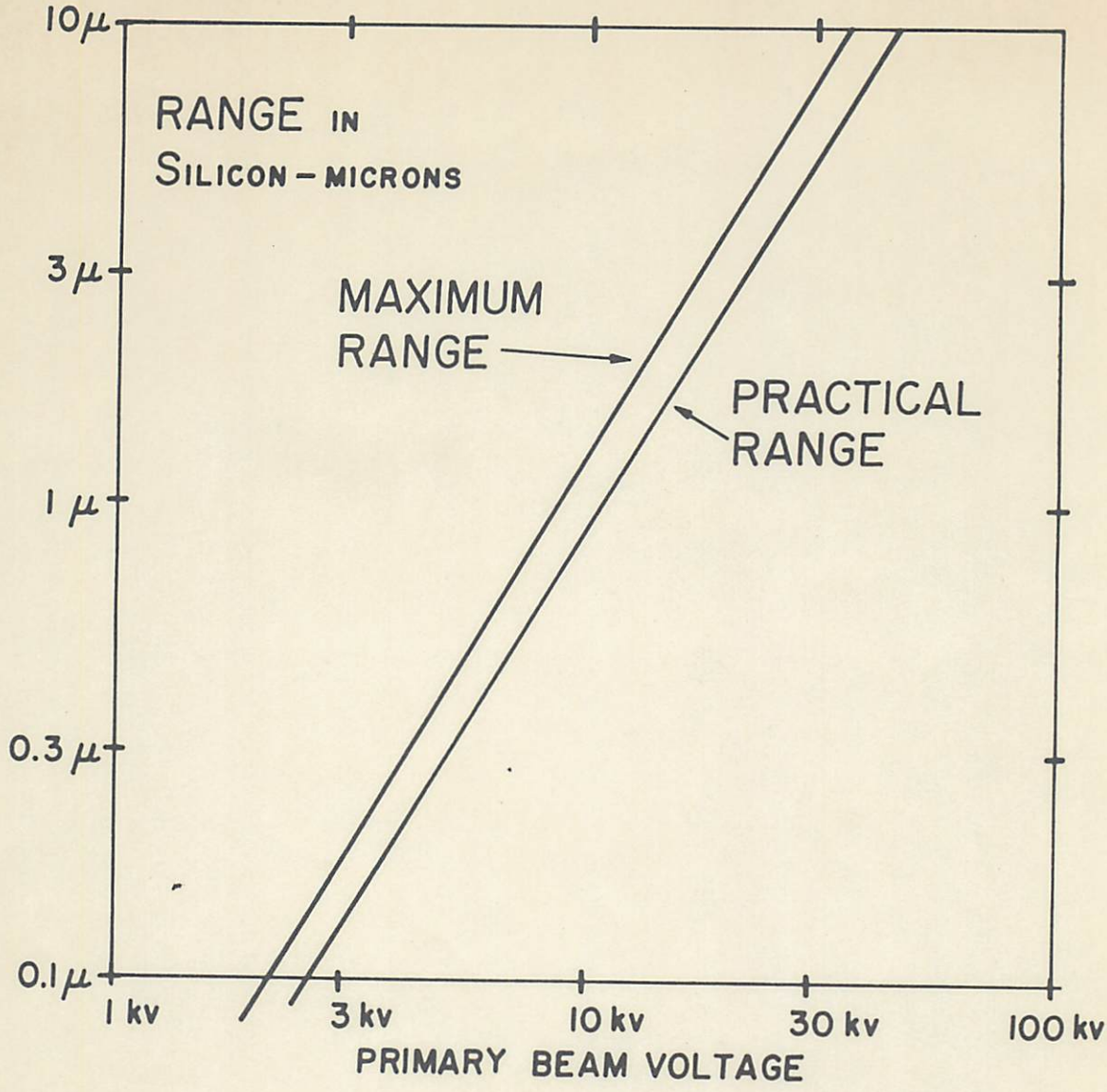
10μ
3μ
1μ
0.3μ
0.1μ
RANGE IN
SILICON – MICRONS
MAXIMUM
RANGE
PRACTICAL
RANGE
1 kv
3 kv
10 kv
30 kv
100 kv
PRIMARY BEAM VOLTAGE

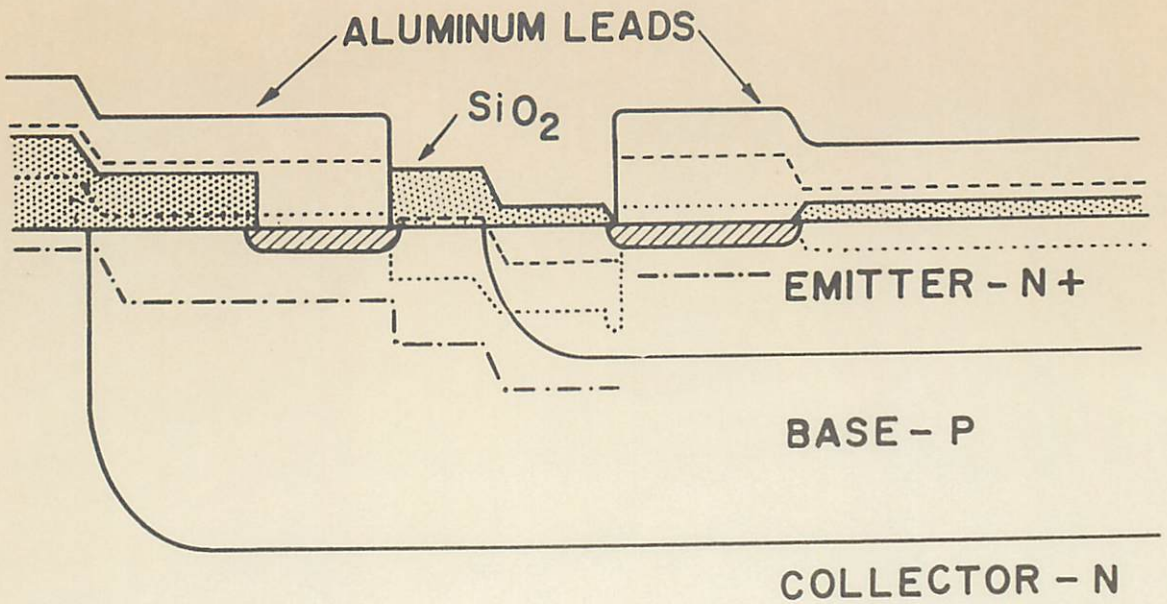

DIMENSIONS - HORIZONTAL, MILS
VERTICAL, MICRONS

PENETRATION DEPTH - V_1 - - - - -, V_2 ·····, V_3 -·-·-

$V_1 < V_2 < V_3$

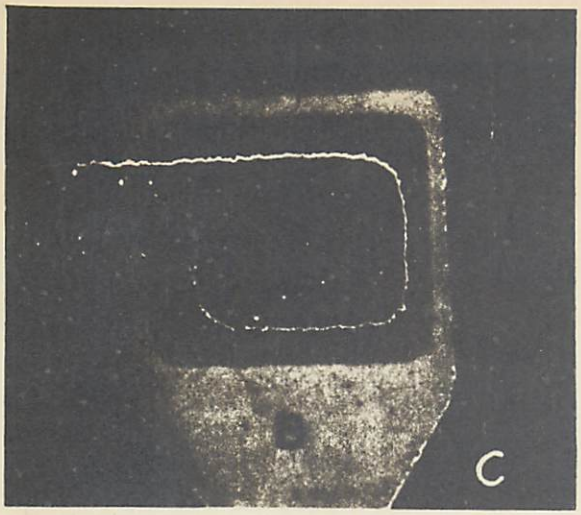

(a) V_B = -1v; V_C = +2v;
V_E = 0v; M = 480
Beam voltage = 16 kv.

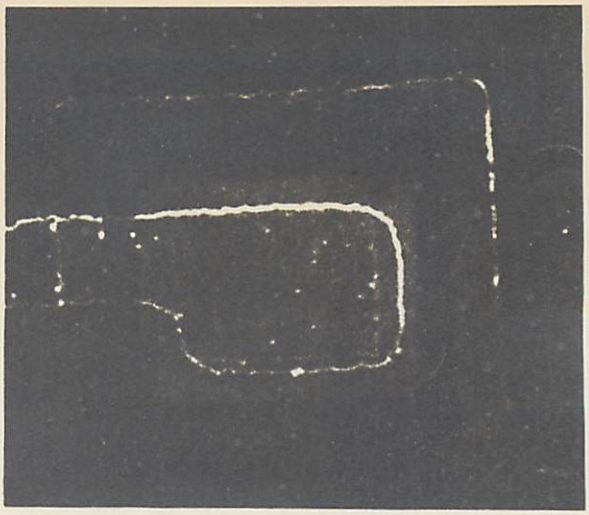

(b) V_B = photovoltage; V_C = +1v.
V_E = 0v;
Beam voltage = 12 kv.

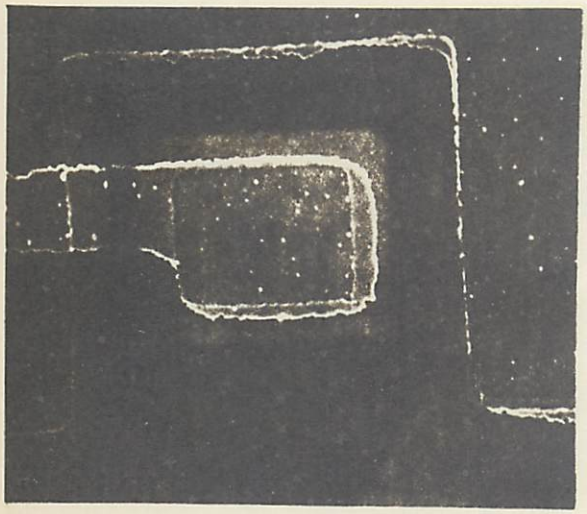

(c) V_B = photovoltage; V_C = +1v
V_E = 0v; M = 480
Beam voltage = 16 kv.

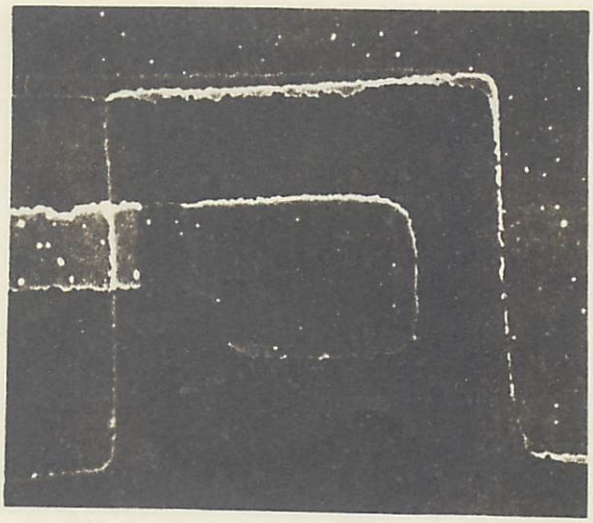

(d) Conditions as (c),
Beam voltage = 20 kv.

Scanning electron micrographs of a commercial functional electronic block.

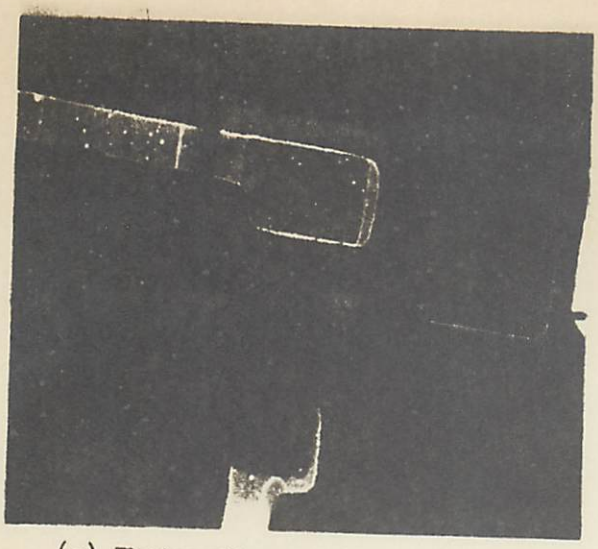

(a) Photovoltage mixed with video signal; collector-emitter reverse-bias = 4v.
Beam voltage = 16 kv. M = 280

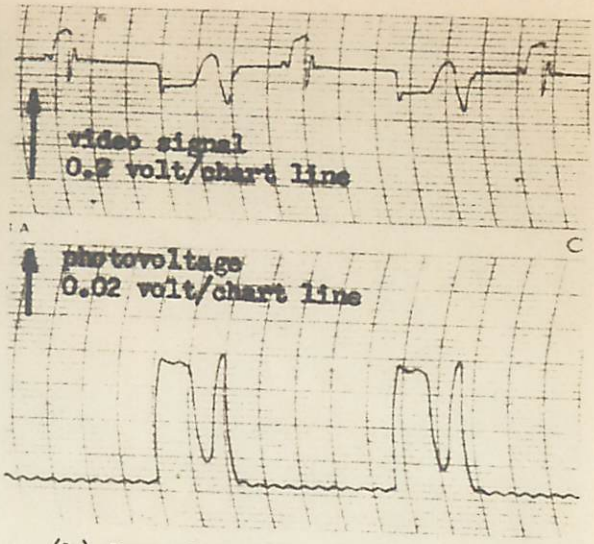

(b) Recorded video waveform and photovoltage of (a) at indicated horizontal line.

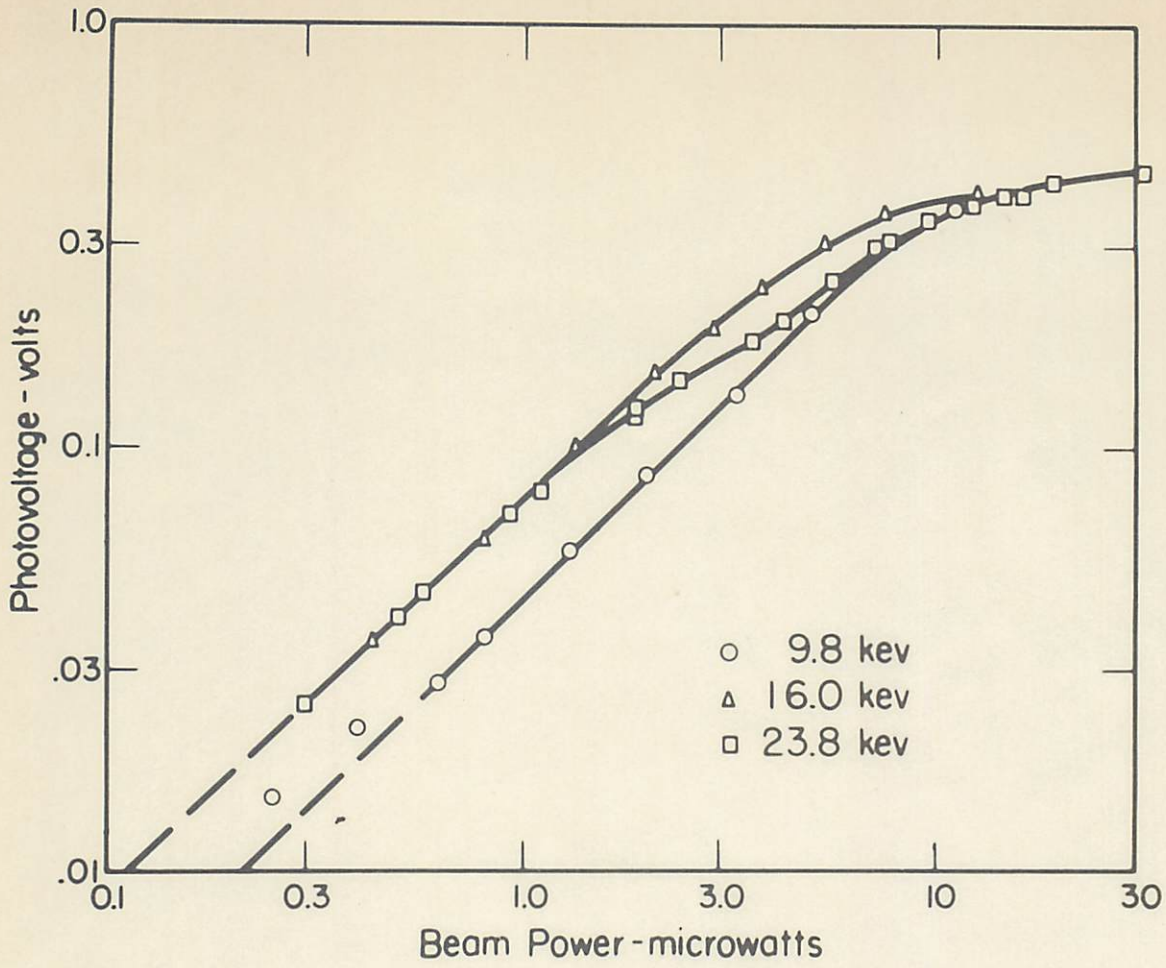
1.0
0.3
0.1
.03
.01
Photovoltage - volts
0.1
0.3
1.0
3.0
10
30
Beam Power - microwatts
○ 9.8 kev
△ 16.0 kev
□ 23.8 kev

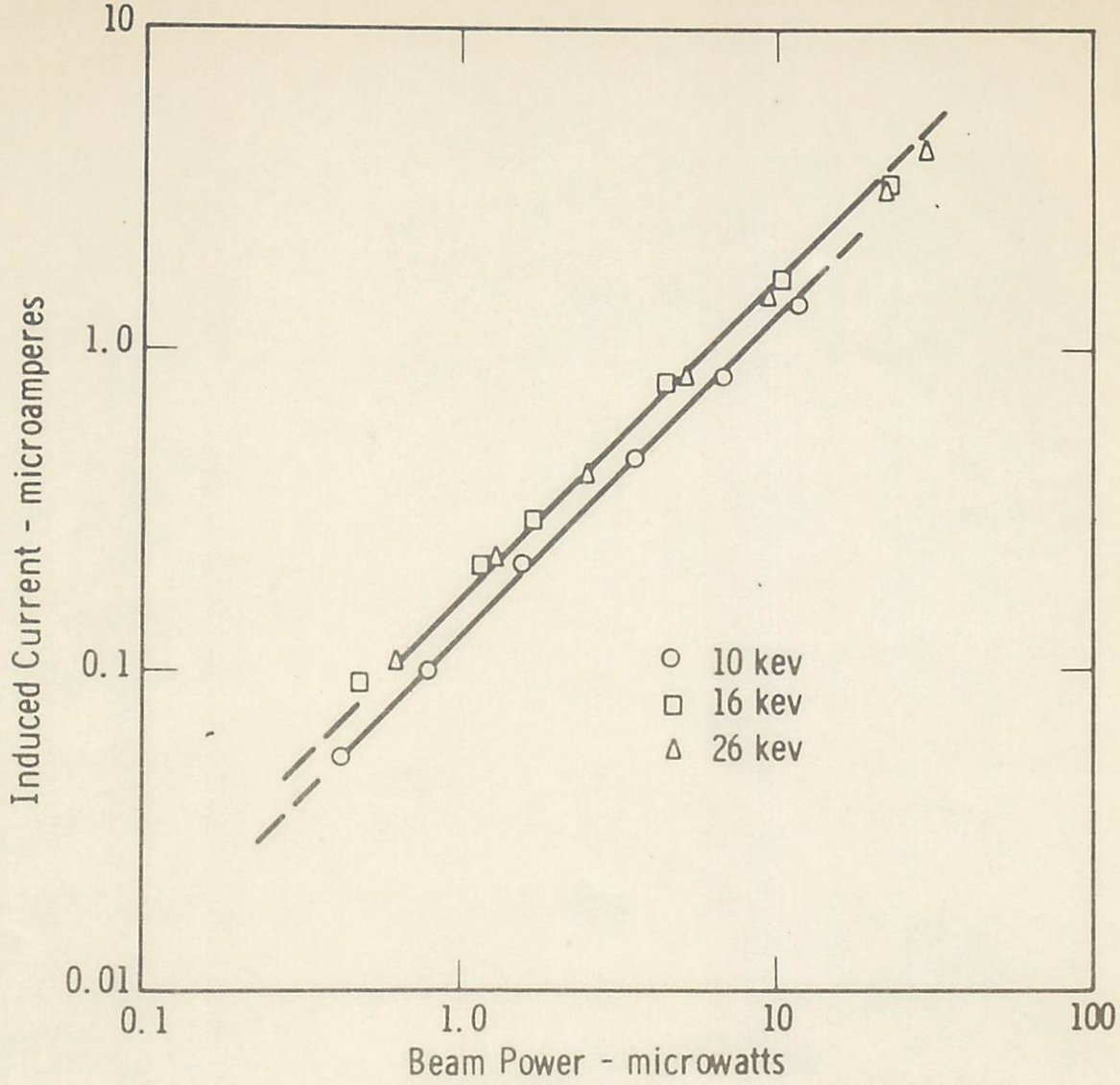
10
1.0
0.1
0.01
Induced Current - microamperes
0.1
1.0
10
100
Beam Power - microwatts
10 kev
16 kev
26 kev

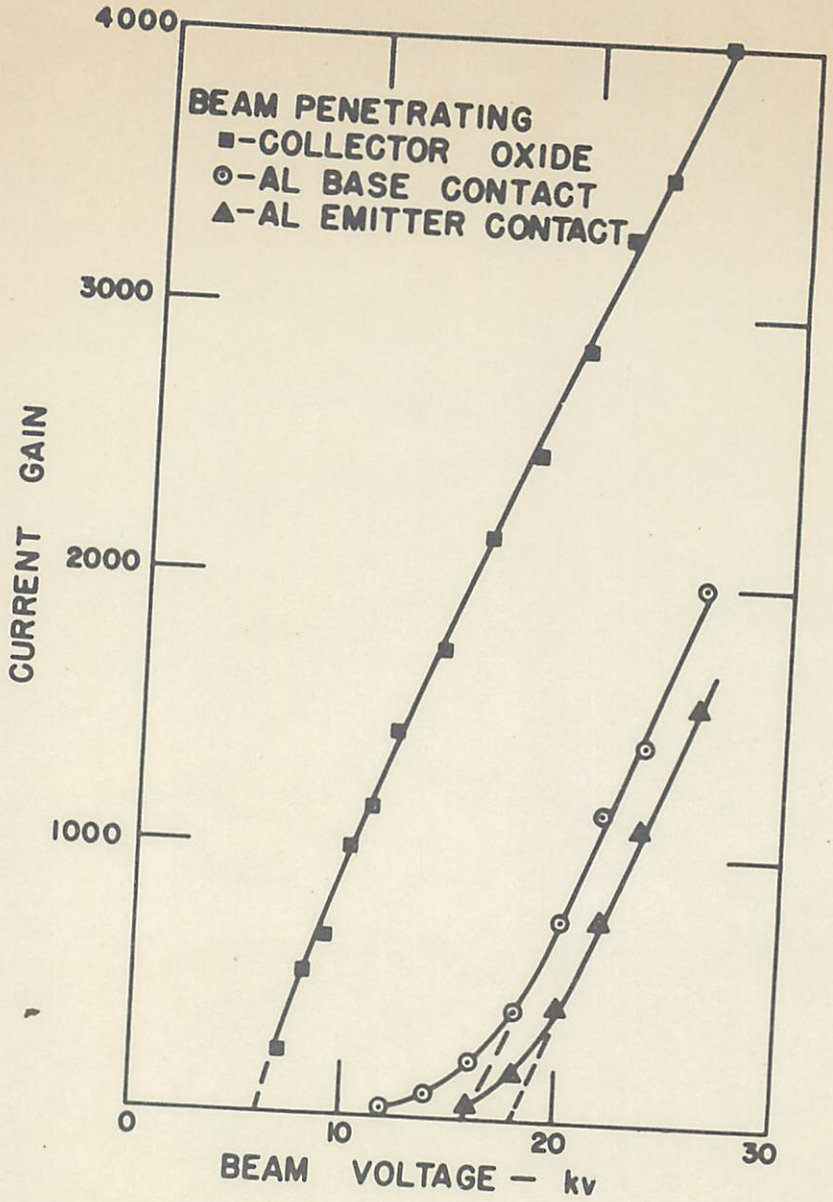
4000
3000
2000
1000
0
10
20
30
CURRENT GAIN
BEAM VOLTAGE — kv
BEAM PENETRATING
■-COLLECTOR OXIDE
⊙-AL BASE CONTACT
▲-AL EMITTER CONTACT

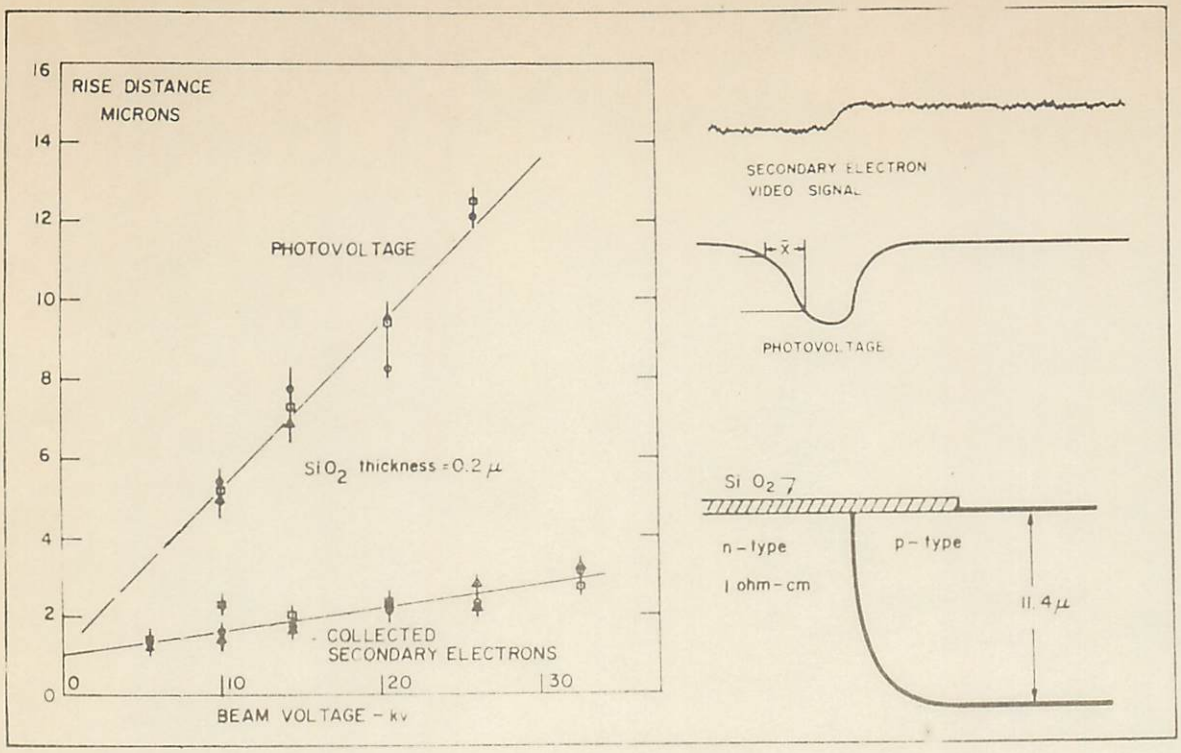
RISE DISTANCE
MICRONS
16
14
12
10
8
6
4
2
0
PHOTOVOLTAGE
SiO_2 thickness = 0.2 μ
COLLECTED
SECONDARY ELECTRONS
0
10
20
30
BEAM VOLTAGE - kv
SECONDARY ELECTRON
VIDEO SIGNAL
x̄
PHOTOVOLTAGE
Si O_2
n - type
1 ohm - cm
p - type
11.4 μ

Fig 3.